Annealing Kinetics of Vacancy Defects in Quenched Gold at Elevated Temperatures*

C. G. WANG,† D. N. SEIDMAN, AND R. W. BALLUFFI
Department of Materials Science and Engineering, Cornell University, Ithaca, New York 14850
(Received 25 September 1967)

A new technique was developed for studying the annealing of supersaturated vacancy defects under comparatively simple conditions at elevated temperatures in gold. A resistance-heated wire specimen mounted in a helium-filled cryostat was (i) gas-quenched from 700°C to an elevated annealing temperature ($180°C \lesssim T_a \lesssim 670°C$) where it was held steady for periods between 100 msec and 10 min; and (ii) quenched to 78°K. The total loss of defects was then obtained from electrical-resistivity measurements at 4.2°K. The temperature-time history was obtained using a rapid-data-acquisition system. The annealing data were consistent with a monovacancy-divacancy annealing model in which the divacancy possessed a migration energy of $E^m=0.69$ eV and a binding energy of 0.40 eV. In addition, the model parameters were consistent with available equilibrium vacancy-defect-concentration data and high-temperature self-diffusion data. The results also agreed with earlier work at lower temperatures by Ytterhus and Balluffi and others in which a defect (evidently the above divacancy) dominated the annealing with $E^m=0.71\pm0.03$ eV. The annealing kinetics were consistent with simple annealing to existing dislocations. Information about the dislocation sink efficiency was also obtained. For $T_a \lesssim 483°C$ the dislocations appeared to act as perfect line sinks present at densities between 0.65 and 5.1×10^7 cm^{-2} in the various specimens. Above $T_a \simeq 600°C$ the sink efficiency apparently decreased because of a decreased driving force for climb.

I. INTRODUCTION

DESPITE a decade of research on the electrical-resistivity annealing of quenched gold, our knowledge of the quenched-in vacancy defects has remained unsatisfactory. The usual procedure has been to quench and then anneal at a sufficiently low temperature to produce an annealing rate which can be measured conveniently. This limitation has restricted the measurements to a relatively narrow range of temperature centered around room temperature. At these comparatively low temperatures there is a strong tendency for the supersaturated vacancy defects to form clusters. The analysis of the annealing kinetics thus becomes a very complex exercise aimed at deducing the individual properties of the different vacancy defect species which contributed to the measured over-all annealing rate. The unsatisfactory status of this experimental situation was indicated clearly at the conference on lattice defects in quenched metals which was held at the Argonne National Laboratory in 1964.[1]

Considerable effort has been made to interpret the results of low-temperature annealing experiments with gold in terms of a relatively simple model involving only monovacancies and divacancies. Koehler and co-workers[2] have interpreted their experiments by employing this model with a divacancy binding energy near $E_{2v}{}^b=0.1$ eV. Seeger and co-workers[3] have also interpreted various experiments in terms of mainly monovacancies and divacancies with $E_{2v}{}^b$ again near 0.1 eV. On the other hand, Westdrop *et al.*,[4] Mori *et al.*,[5] Kauffman and Meshii,[6] and Ytterhus and Balluffi[7] have suggested that the divacancy binding energy may be considerably higher. In particular, Ytterhus and Balluffi found evidence that a vacancy-type defect, with a migration energy of $E^m=0.71$ eV, appeared to dominate the annealing kinetics in quenched gold of nominal 99.999 wt% purity over a wide range of annealing conditions, i.e., at total defect concentrations ranging between $\sim4\times10^{-5}$ and 1×10^{-6} atom fractions, at temperatures between 30 and 185°C, and in specimens with ppm impurity contents differing by factors $<\sim4$. This same migration energy of 0.71 eV was also observed by Mori, Meshii, and Kauffman,[5,6] Siegel,[8] and

* Supported by the U. S. Atomic Energy Commission under Contract No. AT(30-1)3504. Additional support was received from the Advanced Research Projects Agency through the use of the Central Facilities of the Materials Science Center, Cornell University. Parts of this paper were delivered at the American Physical Society Meeting, 30 March 1967 [Bull. Am. Soc. 12, 389 (1967)].

† Department of Applied Physics, Cornell University, Ithaca, N. Y.

[1] See preface and articles in *Lattice Defects in Quenched Metals*, edited by R. M. J. Cotterill *et al.* (Academic Press Inc., New York, 1965).

[2] J. E. Bauerle and J. S. Koehler, Phys. Rev. **107**, 1493 (1957); J. S. Koehler, F. Seitz, and J. E. Bauerle, *ibid.* **107**, 1499 (1957); M. de Jong and J. S. Koehler, *ibid.* **129**, 40 (1963); **129**, 50 (1963); J. S. Koehler, M. de Jong, and F. Seitz, J. Phys. Soc. Japan **18** (Suppl. 3), 1 (1963); T. Kino and J. S. Koehler, Bull. Am. Phys. Soc. **11**, 183 (1966); T. Kino and J. S. Koehler, Phys. Rev. **162**, 632 (1967).

[3] W. Schüle, A. Seeger, D. Schumacher, and K. King, Phys. Status Solidi **2**, 1199 (1962); A. Seeger and D. Schumacher, in *Lattice Defects in Quenched Metals*, edited by R. M. J. Cotterill *et al.* (Academic Press Inc., New York, 1965), p. 15; K. P. Chik, D. Schumacher, and A. Seeger, in *Phase Stability in Metals and Alloys*, edited by P. S. Rudman *et al.* (McGraw-Hill Book Co., New York, 1967), p. 449.

[4] W. Westdorp, H. Kimura, and R. Maddin, Acta Met. **12**, 495 (1964).

[5] T. Mori, M. Meshii, and J. W. Kauffman, Acta Met. **9**, 71 (1961); T. Mori, M. Meshii, and J. W. Kauffman, J. Appl. Phys. **33**, 2776 (1962).

[6] M. Meshii and J. W. Kauffman, Acta Met. **8**, 815 (1960); J. W. Kauffman and M. Meshii, in *Lattice Defects in Quenched Metals*, edited by R. M. J. Cotterill *et al.* (Academic Press Inc., New York, 1965), p. 77.

[7] J. A. Ytterhus and R. W. Balluffi, Phil. Mag. **11**, 707 (1965); J. A. Ytterhus, R. W. Balluffi, J. S. Koehler, and R. W. Siegel, *ibid.* **10**, 169 (1964).

[8] R. W. Siegel, Phil. Mag. **13**, 337 (1966).

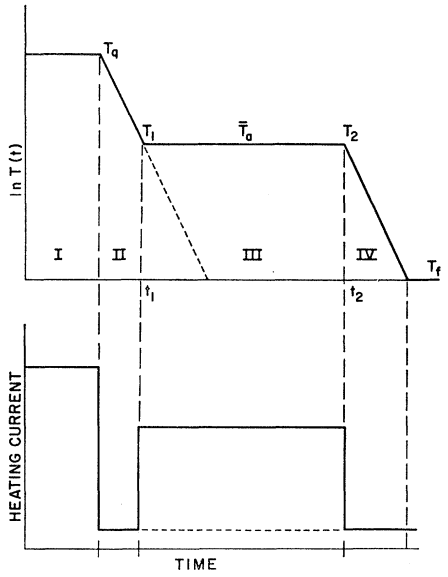

FIG. 1. Upper schematic curve shows $\ln T(t)$ versus time in the four different regions of a typical quenching and annealing run. Region I corresponds to holding at $\bar{T}_q$, region III corresponds to holding at $\bar{T}_a$, while regions II and IV are the transient quenching portions between the nearly isothermal sections. Lower curve represents the time-dependent current waveform necessary to produce $T(t)$.

Delaplace *et al.*[9] Ytterhus and Balluffi[7] tentatively assumed this defect to be the divacancy and concluded that $E_{2v}{}^b$ would have to be greater than about 0.3 eV in order to explain their results. Very recently, Emrick[10] has reported pulse annealing experiments up to 418°C with $E^m=0.67\pm0.07$ eV. He concluded on the basis of this work that divacancies with $E_{2v}{}^b>0.35$ eV dominated the annealing.

The major goal of the present work was to study the annealing of quenched gold over a much wider range of temperature than achieved previously in order to obtain a more critical test of vacancy defect annealing models. For this purpose a new technique was developed which allowed the defect-annealing kinetics to be studied in quenched wires as a function of temperature up to 670°C. In the following we first describe the experimental techniques. The quenching and annealing results are then given, and finally, a possible interpretation of the data is discussed.

II. EXPERIMENTAL PROCEDURE

The basic procedure was to subject a given wire specimen to a series of runs which included (1) straight down-quenches, and (2) runs where the specimen was subjected to a partial quench, an intermediate anneal under almost isothermal conditions at an average temperature $\bar{T}_a$, and a further down-quench to a final lower "freeze-in" temperature T_f. Schematic temperature-time histories are shown in Fig. 1. A highly accurate record of the temperature-time history (as in Fig. 1) was obtained in each case using a high-speed precision apparatus which measured the specimen resistance as a function of time. The temperature-time history was subsequently obtained from known temperature-versus-resistance data. After each run the specimen was further cooled from T_f (liquid-nitrogen temperature) to 4.2°K, where a measurement of the residual resistivity was made to determine the concentration of excess vacancy defects remaining after the entire treatment.

In the present work the annealing temperatures were elevated enough so that significant vacancy precipitation was avoided, and essentially all defect annealing therefore occurred at existing sinks. By varying the quench temperature T_q and the quenching rate in the straight down-quenching experiments, data were obtained for equilibrium defect concentrations at T_q, and also for defect losses to sinks during down-quenching. In the quenching and annealing runs, the emphasis was on measuring the kinetics of the defect loss to sinks during the nearly isothermal anneal at $\bar{T}_a$ (which under the experimental condition employed were almost entirely dislocations[11]). To accomplish this, the defect losses to sinks during the two quenching stages were deduced from data obtained from the straight down-quenching runs. The loss at $\bar{T}_a$ was then obtained by taking differences. By varying $\bar{T}_a$ between 200 and 670°C, and the annealing time between 100 msec and 10 min, a considerable amount of information about the annealing kinetics of the excess defects was obtained as a function of temperature. A typical experimental temperature-time curve is shown in Fig. 2.

A. Specimen

All of the experiments were done with the wire specimens mounted in fixed position in the quenching cryostat shown in Fig. 3. The specimens were resistance heated with a constant dc, and the quenching and annealing runs were carried out in a static atmosphere of helium gas by suitably varying the heating current while keeping the cryostat immersed in liquid nitrogen. All specimen-resistance measurements, under both static conditions and dynamic quenching conditions, were made by passing a measured dc through the

[9] J. Delaplace, J. Hillairet, C. Mairy, and Y. Adda, Mem. Sci. Rev. Met. **63**, 281 (1966).

[10] R. M. Emrick, in *Lattice Defects in Quenched Metals*, edited by R. M. J. Cotterill *et al.* (Academic Press Inc., New York, 1965), p. 91; Bull. Am. Phys. Soc. **12**, 389 (1967); Phys. Letters **25A**, 249 (1967).

[11] In results to be presented later, it will be shown that the dominant sinks during annealing at $\bar{T}_a$ were dislocations. However, during the initial down-quenching additional sinks such as surfaces, grain boundaries, and sub-boundaries undoubtedly played a role in some of the specimens possessing particularly low dislocation densities. This result was due to the greater relative importance of the fast initial transient annealing to a surface or grain boundary sink than to a line sink. This effect may be seen in Fig. 19 and is discussed in Sec. III D.

TABLE I. Specimen data.

Spec.	Specimen purity (wt.% Au)	$\mathfrak{R}_{meas}$ $=R(40°C)/R(4.2°K)$	$\mathfrak{R}_{bulk}$ $=R(40°C)/R(4.2°K)$[a]	$N_d(cm^{-2})$[b]
A	99.999[c]	2311	4612	8.3×10^6
B	99.999[c]	2553	5408	1.0×10^7
C	99.999[c]	1870	3345	1.4×10^7
D	99.9999[d]	3218	7849	5.1×10^7
E	99.999[c]	1844	3287	9.6×10^6
F	99.999[c]	2541	5349	6.5×10^6

[a] Data corrected to eliminate the contribution of surface scattering. We assumed diffuse surface scattering and used the equations of E. H. Sondheimer [Advan. Phys. 1, 1 (1952)] and the experimental value of R. G. Chambers [Proc. Roy. Soc. (London) **A215**, 418 (1952)] for the product of the resistivity and the mean free electron path in order to perform this correction.
[b] Calculated values to fit the two-defect (monovacancy-divacancy) model (see Sec. III C).
[c] Supplied by Sigmund Cohn Corporation.
[d] Supplied by Cominco Products, Inc.

specimen and measuring potentiometrically the voltage drop across the potential leads.

The 0.0127-cm-diam gold wire specimens were made from either nominally 99.999 wt% pure wire from Sigmund Cohn Corporation, or nominally 99.9999 wt% pure wire from Cominco Products, Inc. Specimen data are given in Table I. The potential leads, which were sintered to the specimens, were of 0.00127-cm-diam gold wire of nominal 99.99 wt% purity. Each specimen was first mounted, and then the shapes of the end loops (see Fig. 3) were adjusted in order to obtain a uniform temperature distribution along the gage length at T_q. The specimen was then given a prequench anneal in air at 850–900°C for 10 min in order to reduce and stabilize its dislocation content, stabilize its shape, and increase its purity.[7,8] After annealing, only specimens with purities corresponding to a bulk resistance ratio $\mathfrak{R}=R(40°C)/R(4.2°K)$ of 3000 or greater were used (see Table I).

B. Quenching and Annealing

After the prequench air anneal, the specimen cryostat was evacuated and filled with helium gas. The specimen

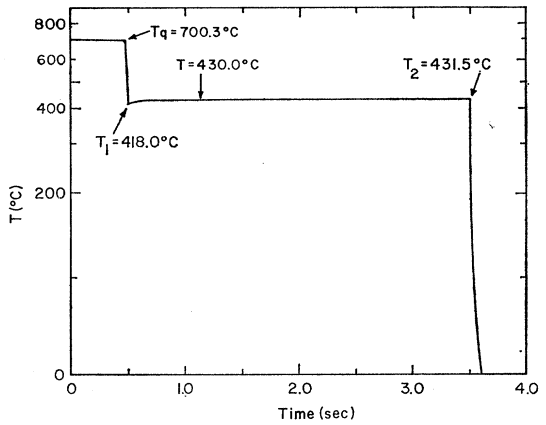

FIG. 2. Actual temperature-time history of a high-temperature anneal. The density of recorded measurements was so high that a smooth curve was drawn through the closely spaced data points.

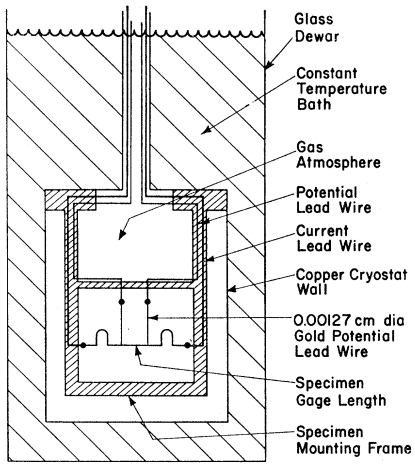

FIG. 3. Schematic cross section of the cryostat containing a mounted specimen. The cryostat is shown immersed in a constant-temperature bath. The cryostat was filled with the quenching gas via the upper cylindrical tube.

resistance at 40.00°C was then measured while keeping the cryostat immersed in a constant-temperature bath maintained at 40.00±0.01°C. This measurement served as a calibration, since all subsequent specimen temperatures were obtained by using the specimen as a resistance thermometer (calibrated at 40.00°C) with a resistance-versus-temperature characteristic given by the data of Meechan and Eggleston.[12] All static resistance measurements were made using the standard dc potentiometric method described, for example, by Ytterhus and Balluffi.[7] Resistance changes accurate to better than $10^{-8}\,\Omega$ were measured. In order to either quench, or quench and anneal, the cryostat was immersed in liquid nitrogen, and the specimen was heated to T_q (close to 700°C in the present work) and held for 5 min. The heating current was then reduced abruptly to a small value for a straight down-quench, or else varied (as shown in Fig. 1) in order to produce the desired temperature-time behavior for a quench and anneal run. The current was never completely turned off, since it was always necessary to have a small measuring current to monitor the specimen resistance. The specimen cooled exponentially during the quenching periods according to

$$T(t)=T_f+(T_q-T_f)\exp(-Bt). \qquad (1)$$

With $T_q=700°C$, $T_f=-195°C$, and $B=8.0\ sec^{-1}$, an initial quenching rate of $\simeq 7200°C\ sec^{-1}$ was achieved.

The specimen resistance during the runs was obtained potentiometrically by measuring in a differential mode, at high speed, the voltage drops across the specimen and across a standard resistor in series with the specimen. Both analog signals were fed to a pair of amplifiers as seen in Fig. 4.[13] During an isothermal stage, the ampli-

[12] C. J. Meechan and R. R. Eggleston, Acta Met. 2, 680 (1954).
[13] See Appendix A for further discussion of the measuring and recording apparatus.

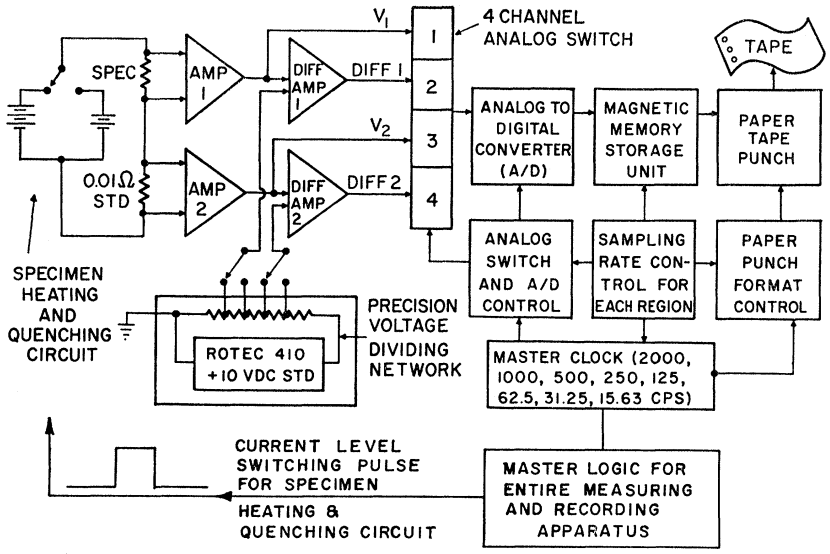

FIG. 4. Schematic diagram of the rapid measuring data acquisition system. The details of the circuit are discussed in Appendix A.

fied analog signals were compared with the preadjusted and calibrated reference voltages. Any differences were next fed into another pair of differential amplifiers. The amplified analog signals from the second pair of amplifiers (for isothermal stages) or from the first pair of amplifiers (for straight down-quenches) were digitized and stored in a half-cycle memory core unit. The memory unit then released the information to a paper tape punch. The paper tape was then decoded using a computer. A computer program was used to convert the data to specimen resistance and then to specimen temperature. In this manner the temperature-time history was measured at a frequency of up to 4×10^3 readings sec^{-1}. For the isothermal stages, the uncertainty in the temperature measurement was less than 0.5°C.

Each specimen was quenched and annealed a considerable number of times in order to obtain a self-consistent set of annealing data for each specimen over a wide range of temperatures. Since essentially all the annealing occurred at existing sinks, it was necessary to keep the sink density as constant as possible during all of the runs for a given specimen and to verify this result experimentally. This was done by setting the quenching temperature T_q fairly low (700°C), and by carrying out a straight down-quench run between every two or three quench and anneal runs. The thermal history during the down-quench and the defect losses were highly reproducible. Measurements of the quenched-in increments upon straight down-quenching were therefore used continuously as an index of possible changes in the specimen sink density. The measurements also served as a continuous calibration of the entire quenching and measuring technique. The results of these check runs (see below) indicated that the sink density remained constant in a given specimen to better than about 6%. The following features of the present technique aided in achieving this goal: (1) The *in situ* mounting eliminated specimen handling; (2) the large loops at the specimen ends (Fig. 3) allowed free longitudinal thermal expansion; (3) after the initial stabilizing anneal, the wire was supported against subsequent sagging at high temperatures by the two potential lead wires (Fig. 3), and visual inspection showed no perceptible change in specimen shape after the initial stabilizing anneal; and (4) the helium gas quench was relatively slow and gentle compared to, for example, a fast liquid quench.[14] In fact, the annealed resistance of each specimen at 40.00°C remained constant during all subsequent treatments to better than a few parts in 10^5.

Between each quenching treatment the specimen was always subjected to an anneal of several minutes at 700°C. This served to anneal out any defects or unstabilized sink structure remaining after the previous quench. The residual annealed resistance at 4.2°K was also monitored at suitable intervals in the series of quenching treatments. For this measurement the specimen was very slowly cooled from 700°C in order to eliminate any excess vacancy defects. These measurements established a base resistance which served to reveal any unusual changes in the impurity content or dislocation structure.

III. EXPERIMENTAL RESULTS

A. Quenching Experiments

A number of straight down-quenching experiments were performed in order to establish the quenching technique and to gain information about defect losses to sinks during the quenches. All of the experiments in the present investigation were done with $T_q \lesssim 700$°C.

[14] J. J. Jackson, in *Lattice Defects in Quenched Metals*, edited by R. M. J. Cotterill *et al.* (Academic Press Inc., New York, 1965), p. 479.

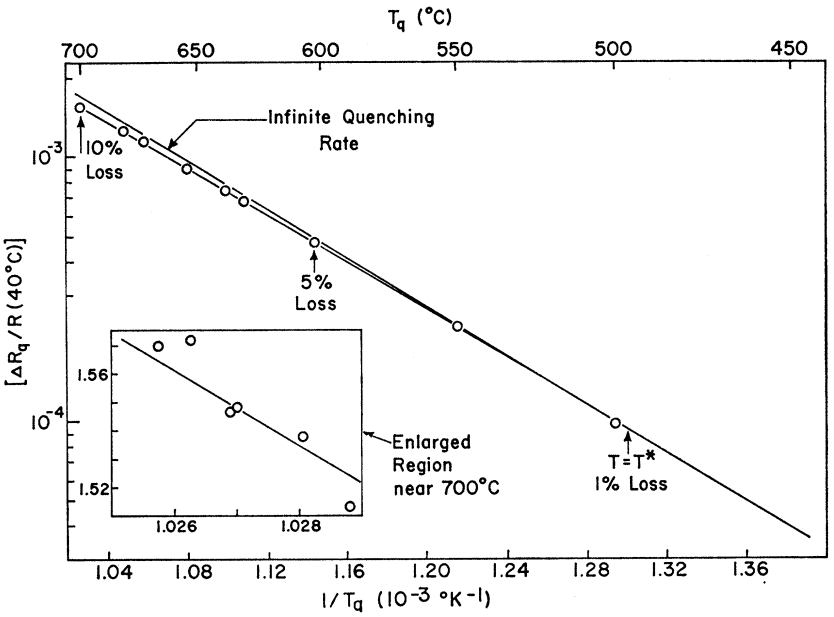

FIG. 5. Typical Arrhenius plot of the quenched-in vacancy-defect resistance increment normalized to $R(40°C)$ for specimen C. The solid line is the resistance increment for an infinitely rapid quenching rate. The inset is an enlarged region near $T_q=700°C$ which serves to indicate the scatter of the data.

At higher temperatures serious temperature instabilities appeared, and it became difficult to hold the specimen temperature constant in the helium atmosphere (this same phenomenon has been reported by Bass,[15] and Flynn, Bass, and Lazarus[15]).

Highly reproducible quenched-in vacancy concentrations were obtained for a given specimen even after it had been used for a number of different quenching and annealing runs. Some results for specimen C are shown in Fig. 5. The enlarged region shows the increments which were obtained after six different quenches from near 700°C which were made at different stages of the specimen's use. Several quench-anneal runs were made between each of the quenches corresponding to the data points shown. The deviations of the increments in Fig. 5 were of the order of 1% or less, from which we concluded that variations in the specimen sink density during its use were small. Results given below established that about 10% of the vacancies were lost during down-quenching in specimen C. Similar results were obtained with other specimens.

The defect losses during quenching from 700°C in several specimens were determined directly by quenching them at different rates and extrapolating the quenched-in increments to an infinitely fast quenching rate as shown, for example, in Fig. 6. The different rates were obtained by using various quenching gas mixtures of helium and nitrogen at different pressures. The extrapolated quenched-in increments are seen to converge fairly well to a common mean value. The extrapolated values show a mean deviation of several percent for the different specimens used. This deviation, while comparatively small, is appreciably larger than the mean deviations obtained from experiments with individual specimens as shown by the self-consistency of the data for individual specimens in Figs. 5 and 6.

The quenched-in increment extrapolated to infinite quenching rate for specimen C is shown in Fig. 5 as a function of temperature. The 10% loss at T_q was obtained experimentally as explained above. The 5% loss at $T_q=600°C$ and the 1% loss at $T_q=500°C$ are calculated values which were obtained using the monovacancy-divacancy annealing model to fixed sinks described later in Sec. III C. In this model first-order annealing to a constant density of sinks is assumed. The calculation employed the monovacancy-divacancy parameters deduced in Sec. III C and listed in Table II. A constant effective sink density for all the down-quenches was calculated using the measured loss of 10% for the quench from 700°C as a calibration value. However, the assumption of first-order kinetics was not strictly accurate for several of the present specimens

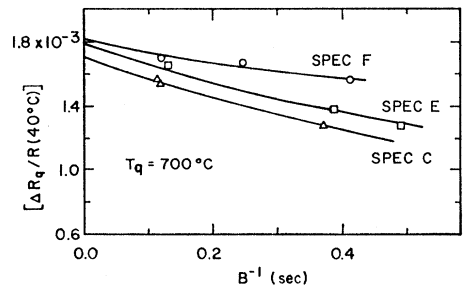

FIG. 6. Quenched-in vacancy-defect resistance increment normalized to $R(40°C)$ versus the quenching rate constant B^{-1} for specimens C, E, and F. The experimental points are indicated by crosses, squares, and circles, respectively.

[15] J. Bass, Ph.D. thesis, University of Illinois, 1964 (unpublished); J. Bass, Phys. Rev. **137**, A765 (1965); C. P. Flynn, J. Bass, and D. Lazarus, Phil. Mag. **11**, 521 (1965).

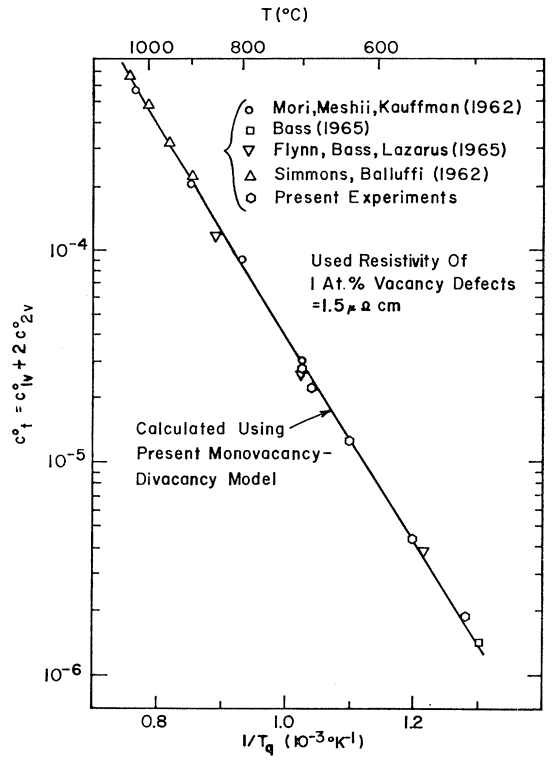

FIG. 7. Arrhenius plot of the equilibrium total vacancy concentration versus reciprocal temperature based on all available experimental data. The high-temperature points were obtained from the direct absolute measurements of Simmons and Balluffi (Ref. 16), while the remaining points were obtained by extrapolating the quenched-in vacancy resistivity increments to infinite quenching rate and then converting them to concentration using a defect resistivity of 1.5 $\mu\Omega$ cm (at.%)$^{-1}$. The solid line is a calculated curve employing the present monovacancy-divacancy model with the parameters listed in Table II.

which contained particularly low dislocation densities. In these specimens some annealing during quenching must have occurred to grain boundary and surface sinks. While first-order annealing is expected to dislocations, the annealing to grain boundaries or surfaces is not expected to be of first order. The situation is shown in Fig. 19, where simplified calculations of upper limits of the annealing to the various possible sinks are presented. The calculations of the annealing to grain boundaries and surfaces are based on measured densities of these sinks in the specimens used. It is seen that the annealing to these sinks exhibit a relatively rapid transient at small fractional losses which is significant in comparison to the annealing rate to the dislocations. Since these losses do not obey first-order annealing, the assumption in the above calculation of first-order annealing is an approximation. However, since the losses were small this approximation was reasonable. Further discussion is given in Sec. III D. It is shown in Fig. 5 that the losses at temperatures below about 500°C were negligible.

TABLE II. Values of the eight defect parameters derived for the monovacancy-divacancy defect model. $D_{01v}=a^2\nu_{1v}^0\exp(S_{1v}^m/k)$; $D_{02v}=\frac{1}{6}a^2\nu_{2v}^0\exp(S_{2v}^m/k)$; $\nu_{1v}^0\exp(S_{1v}^m/k)=4\times10^{13}$ sec$^{-1}\equiv$monovacancy frequency factor; $\nu_{2v}^0\exp(S_{2v}^m/k)=1.37\times10^{13}$ sec$^{-1}\equiv$divacancy frequency factor.

Parameter	Symbol	Best value
1. Monovacancy migration energy	E_{1v}^m	0.90 eV
2. Divacancy migration energy	E_{2v}^m	0.69 eV
3. Monovacancy diffusivity pre-exponential factor	D_{01v}	6.35×10^{-2} cm^2 sec^{-1}
4. Divacancy diffusivity pre-exponential factor	D_{02v}	3.65×10^{-3} cm^2 sec^{-1}
5. Monovacancy formation energy	E_{1v}^f	0.94 eV
6. Divacancy binding energy	E_{2v}^b	0.40 eV
7. Monovacancy formation energy	S_{1v}^f	$0.74k$
8. Divacancy binding entropy	S_{2v}^b	$-0.093k$

In Fig. 7 we present a collection of all of the data which are available to us from various sources which should represent the total equilibrium concentration of vacant lattice sites at temperatures up to the melting point. The high-temperature points of Simmons and Balluffi[16] were obtained from measurements of specimen length and lattice parameter under equilibrium conditions and represent values of the total absolute concentration of vacant lattice sites. The remaining data were all obtained from resistivity quenching experiments where the quenched-in increments were obtained by extrapolation to infinite quenching rates. The corresponding concentrations were calculated from these data using $1.5\times10^{-6}\ \Omega$ cm as the resistivity of 1 at.% of vacant sites. This value is seen to produce a smooth grafting together of the high-temperature absolute measurements of Simmons and Balluffi and the remaining resistivity data. Wherever necessary the data were converted to a common temperature scale corresponding to the resistance-versus-temperature data of Meechan and Eggleston.[12] The various data are seen to be in quite good agreement.

B. Defect Annealing in the Range $\bar{T}_A<500$°C

We now show that the annealing in the range $\bar{T}_A<500$°C appears to be consistent with a defect migrating with $E^m=0.69$ eV. However, we shall see that such a defect by itself cannot explain tracer self-diffusion data in gold near the melting point. This will lead us to the conclusion that at least two important vacancy-type defects must be operative in quenched gold. A relatively simple monovacancy-divacancy annealing model which is consistent with all the available data is then developed in Sec. III C.

Measurements were made of the defect losses to sinks during nearly isothermal anneals at $\bar{T}_a$ between t_1 and t_2 (region III in Fig. 1). The annealing losses were determined directly for temperatures up to $\bar{T}_a\simeq500$°C by measuring on the same specimen: (1) the excess resistance increment ΔR_q due to the quenched-in vacancies obtained by a direct down-quench from T_q;

[16] R. O. Simmons and R. W. Balluffi, Phys. Rev. **125**, 862 (1962).

and (2) the excess resistance increment ΔR_{qa} due to the excess vacancies remaining after a quench and anneal run. As pointed out previously, negligible defect losses occurred during the present quenches at temperatures below about 500°C. Therefore, for runs where $\bar{T}_a < 500$°C, the quantity ΔR_q was proportional to the excess defect concentration $\Delta c(t_1)$, at the beginning of the anneal at $t=t_1$, and the quantity ΔR_{qa} was proportional to the excess vacancy concentration at the end of the anneal at $t=t_2$ (see Fig. 1). Therefore,

$$\frac{\Delta R_q}{\Delta R_{qa}}=\frac{\Delta R(t_1)}{\Delta R(t_2)}=\frac{\Delta c(t_1)}{\Delta c(t_2)}. \tag{2}$$

Under typical conditions the temperature variation between t_1 and t_2 was <30°C. In order to analyze the annealing during this period, taking into account this variation of temperature, we employed a treatment giving the defect loss expressed as an integral of the annealing rate where the variation of temperature with time is included.

Assuming for the present that a single defect dominates the annealing, we may express the annealing rate to sinks rather generally as

$$\frac{d(c-c^0)}{dt}=-f(c-c^0)(c-c^0)D(t), \tag{3}$$

where c is the defect concentration, c^0 is the concentration in equilibrium with the sinks, and $D(t)$ is the time-dependent defect diffusivity. Here, for example, $f(c)$ may be a sink efficiency[17] which varies as annealing proceeds, or it may represent a variation in the effective sink concentration. When c^0 may be neglected in comparison to c, Eq. (3) may be integrated in the following form:

$$\int_{\Delta c(t_1)}^{\Delta c(t_2)}\frac{dc}{f(c)c}=-\int_{t_1}^{t_2}D(t)dt =-D_0\int_{t_1}^{t_2}\exp[-E^m/kT(t)]dt, \tag{4}$$

where D_0 is the usual preexponential diffusivity constant. The solution of Eq. (4) is, in general,

$$g[\Delta c(t_2),\Delta c(t_1)] =-D_0\int_{t_1}^{t_2}\exp[-E^m/kT(t)]dt=-D_0I, \tag{5}$$

where I represents the integral of the time-dependent Boltzmann factor. For the present case of monotonic annealing we would expect that

$$\ln[\Delta c(t_1)/\Delta c_2(t)]=\ln(\Delta R_q/\Delta R_{qa})=\phi(I), \tag{6}$$

[17] R. W. Balluffi and R. W. Siegel, in *Lattice Defects in Quenched Metals*, edited by R. M. J. Cotterill *et al.* (Academic Press Inc., New York, 1965), p. 693.

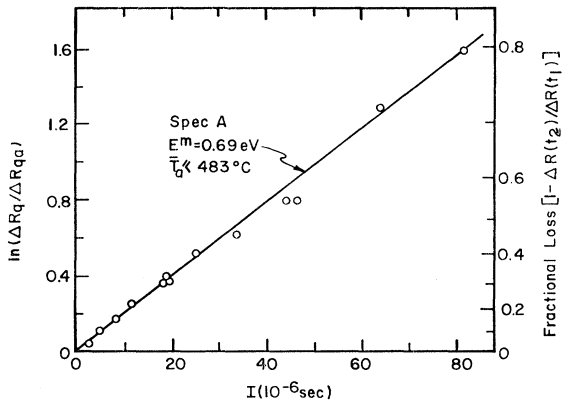

FIG. 8. $\ln(\Delta R_q/\Delta R_{qa})$ (left-hand ordinate) versus the integral I defined in Eq. (5) for specimen A. This plot yielded a migration energy of 0.69 eV for $\bar{T}_a \leq 483$°C. The right-hand ordinate indicates the corresponding fractional vacancy loss.

where ϕ is some monotonic function of I. For the case of first-order annealing to fixed dislocation sinks at a constant density and unit sink efficiency[18] Eq. (6) takes the form

$$\ln[\Delta c(t_1)/\Delta c(t_2)]=\ln[\Delta R_q/\Delta R_{qa}]=G(N_d)D_0I=AI, \tag{7}$$

where

$$G(N_d)=-2\pi N_d/\ln[r_d(\pi N_d)^{1/2}]. \tag{8}$$

Here N_d is the dislocation density and r_d is the dislocation capture radius for defects.

We may also define $\bar{T}_a$ by the equation

$$[t_2-t_1]\exp[-E^m/k\bar{T}_a]=\int_{t_1}^{t_2}\exp[-E^m/kT(t)]dt, \tag{9}$$

so that $\bar{T}_a$ is the best average temperature which describes the annealing between t_1 and t_2.

The best value of E^m for the present annealing experiments with $\bar{T}_a<500$°C was found by applying the experimental data to Eq. (6) using a computer in order to evaluate the integral by Simpson's rule. Measurements of ΔR_q, ΔR_{qa}, and $T=T(t)$ were available for each quench and anneal in the series of runs performed on each specimen. The *only unknown* in Eq. (6) was then E^m, which appears in the integral I. The best value of this quantity was found by determining the particular value of E^m which caused all the values of $(\Delta R_q/\Delta R_{qa})$ for a given specimen to give a best fit to a smooth curve on a plot of $\ln(\Delta R_q/\Delta R_{qa})$ versus I. The results for specimens A, B, and D are shown in Figs. 8 and 9, where best fits were obtained with E^m values in the range 0.66–0.69 eV. The value of E^m which produced this fit was very sharply defined. This is shown

[18] As previously mentioned, essentially all the annealing occurred at dislocations during the anneals at T_a, since by this time any early rapid transients to the surfaces and grain boundaries had decayed (see Sec. III D and Fig. 19). Also, see Sec. III D for a definition of unit sink efficiency.

in Fig. 10 where we have plotted the fractional standard deviation of the points from the various smooth curves in the plots which were obtained for specimens A and D using different assumed values of E^m. The well-defined minima in the plots of the fractional standard deviation as a function of E^m (Fig. 10) correspond to $E^m=0.69$ and 0.66 eV for specimens A and D, respectively. The nearly straight lines obtained in the plots in Figs. 8 and 9 indicate that the annealing was approximately first order according to Eq. (7). The results therefore appear to be consistent with an annealing model in which a vacancy defect with $E^m=0.69$ eV annealed to fixed dislocation sinks. Estimates of the required dislocation densities showed that they were close to the values which would be expected from the previous direct measurements by Seidman and Balluffi.[19]

Further determinations of E^m were made by another method. If we assume first-order kinetics and use Eqs. (7) and (9) we obtain

$$1/(t_2-t_1)\ln(\Delta R_q/\Delta R_{qa})=A\exp(-E^m/k\bar{T}_a). \quad (10)$$

A plot of $\ln[1/(t_2-t_1)\ln(\Delta R_q/\Delta R_{qa})]$ versus $1/\bar{T}_a$ should therefore yield a straight line of slope proportional to E^m. Values of $\bar{T}_a$ were obtained with the computer, and the results, which span three logarithmic decades, are shown in Fig. 11. Values of E^m near 0.69 eV were again obtained in agreement with the previous results.

We may conclude that the results up to this point for the annealing in the temperature range 200 to ~500°C are consistent with one type of defect which migrates to dislocation sinks with a migration energy of 0.69 eV. However, it is readily shown that this defect by itself is not capable of explaining all of the vacancy defect

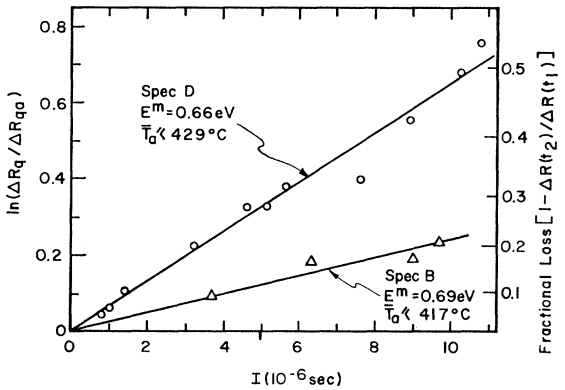

FIG. 9. $\ln(\Delta R_q/\Delta R_{qa})$ (left hand ordinate) versus the integral I defined in Eq. (5) for specimens B and D. This plot yielded $E^m=0.66$ eV for $\bar{T}_a\leq 424$°C for specimen D, and $E^m=0.69$ for $\bar{T}_a\leq 417$°C for specimen B. The corresponding fractional vacancy loss is plotted on the right-hand ordinate.

[19] D. N. Seidman and R. W. Balluffi, Phys. Rev. **139**, A1824 (1965); D. N. Seidman and R. W. Balluffi, Phys. Status Solidi **17**, 531 (1966); D. N. Seidman and R. W. Balluffi, in *Interactions Between Lattice Defects*, edited by R. R. Hasiguti (Gordon and Breach Science Publishers, Inc., New York, 1968), p. 913.

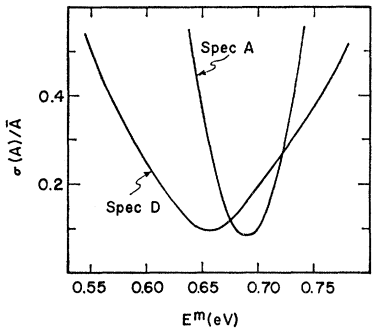

FIG. 10. Fractional standard deviation of the parameter A defined by Eq. (7) from a smooth curve for various values of E^m. The sharply defined minima correspond to the best value of E^m by this method for specimens A and D.

data available to us over all temperatures ranging up to the melting point. Any defect model for gold must account for at least the following:

(i) the defect annealing losses during annealing measured over the full temperature range of the present work (Fig. 13);

(ii) the magnitudes of the thermal equilibrium defect concentrations over the range of temperature shown in Fig. 7;

(iii) the high-temperature tracer self-diffusion data shown in Fig. 12.

The tracer self-diffusion data shown in Fig. 12 were selected from the literature. There have been nine independent determinations[20–28] of the tracer self-diffusion coefficient in gold (see Table III). From a study of the experimental techniques and data of these investigations it was clear that the work of Makin *et al.*,[26] Duhl *et al.*,[27] and Gilder and Lazarus[28] were the most carefully performed experiments. Their values of D_0^{sd} and Q are seen to be in close agreement. It is also noted that Mallard *et al.*[29] measured self-diffusion coefficients for gold in a series of gold-silver alloys and that their extrapolated value of the diffusion coefficient for gold in pure gold is consistent only with the values obtained in Refs. 26–28. The results of those three investigations were therefore selected and are reproduced in Fig. 12.

A few initial calculations showed that (i), (ii), and (iii) could not be satisfactorily explained by a single

[20] A. M. Sagrubskii, Physik Z. Sowjetunion **12**, 118 (1937).
[21] H. A. C. McKay, Trans. Faraday Soc. **34**, 845 (1938).
[22] H. C. Gatos and A. Azzam, J. Metals **4**, 407 (1952).
[23] H. C. Gatos and A. D. Kurtz, J. Metals **6**, 616 (1954).
[24] B. Okkerse, Phys. Rev. **103**, 1246 (1956).
[25] H. W. Mead and C. E. Birchenall, Trans. AIME **209**, 874 (1957).
[26] S. M. Makin, A. H. Rowe, and A. D. LeClaire, Proc. Phys. Soc. (London) **B70**, 545 (1957).
[27] D. Duhl, K. Hirano, and M. Cohen, Acta Met. **11**, 1 (1963).
[28] H. M. Gilder and D. Lazarus, J. Phys. Chem. Solids **26**, 208 (1965).
[29] W. C. Mallard, A. B. Gardner, R. F. Bass, and L. M. Slifkin, Phys. Rev. **129**, 617 (1963).

TABLE III. Self-diffusion data for Au.

Investigator	Year	D_0^{sd} (cm² sec⁻¹)	Q (eV)	Temperature range (°C)
Sagrubskii[a]	1937	0.16	2.3	800–1000
McKay[b]	1938	0.02	2.2	721– 966
Gatos and Azzam[c]	1952	[j]	1.95	800–1000
Gatos and Kurtz[d]	1954	0.065	1.96	680–1060
Okkerse[e]	1956	0.031	1.71	600– 954
Mead and Birchenall[f]	1957	0.14	1.86	717– 992
Makin *et al.*[g]	1957	0.091	1.81	704–1048
Duhl *et al.*[h]	1963	0.117	1.82	702– 889
Gilder and Lazarus[i]	1965	0.107	1.83	850–1050

[a] See Ref. 20.
[b] See Ref. 21.
[c] See Ref. 22.
[d] See Ref. 23.
[e] See Ref. 24.
[f] See Ref. 25.
[g] See Ref. 26.
[h] See Ref. 27.
[i] See Ref. 28.
[j] No value cited.

type of vacancy defect migrating with $E^m=0.69$ eV. We were therefore forced to consider a more complex defect model consisting of at least two different types of defects. The most natural assumption was to assume that the dominant defect at the very highest temperatures near the melting point was the monovacancy and that one (or more) clusters with a positive binding energy become important at lower temperatures. In the following subsection we therefore interpret the data on the basis of the simplest possible model capable of explaining the data listed above under (i), (ii), and (iii), that is, a model consisting of only monovacancies and divacancies.

C. Monovacancy-Divacancy Annealing Model

We assume, as before, that the only sinks during the nearly isothermal annealing period are dislocations, and

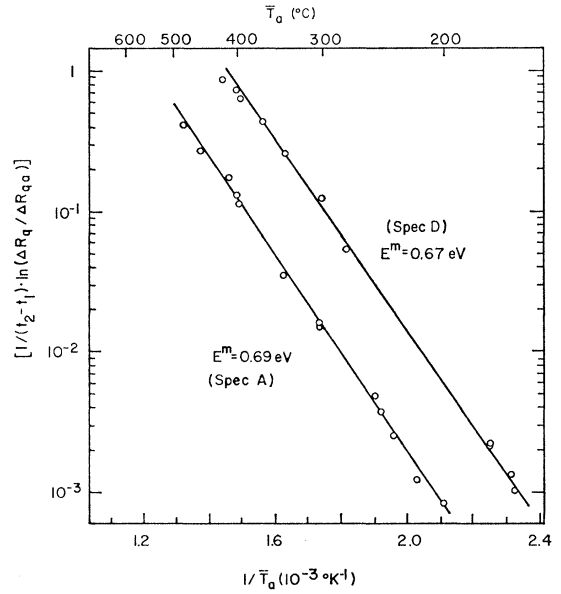

FIG. 11. Plot of $1/(t_2-t_1)\ln(\Delta R_q/\Delta R_{qa})$ versus $\bar{T}_a^{-1}$. These curves yielded activation energies of 0.69 and 0.67 eV for specimens A and D, respectively.

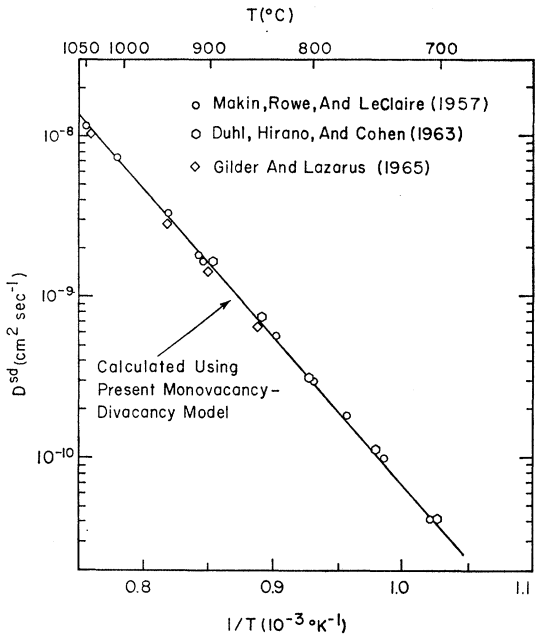

FIG. 12. Arrhenius plot of the self-diffusion coefficient D^{sd} versus T^{-1} for three selected published experimental sets of data. The solid line is the value of D^{sd} calculated from Eqs. (21)–(23) on the basis of the present monovacancy-divacancy model employing the parameters listed in Table II.

that local equilibrium between the monovacancies and divacancies is established so rapidly that we can assume local defect equilibrium at all times. (A justification of this local-equilibrium assumption is given below.) Furthermore, we assume that the dislocations act as sufficiently good sinks so that they maintain the defects in thermal equilibrium in their direct vicinity. Under these conditions the annealing rate to the fixed sinks is diffusion controlled, and it is readily shown, using the results of Flynn[30] and Balluffi and Seidman,[31] that the quasi-steady-state annealing rate under isothermal conditions at $\bar{T}_a$ is then

$$\frac{dc_t}{dt}\simeq -G(N_d)\{D_{1v}(c_{1v}-c_{1v}^0)+2D_{2v}(c_{2v}-c_{2v}^0)\}, \quad (11)$$

where

$$c_t=c_{1v}+2c_{2v}, \quad (12)$$

$$c_{1v}^0=\exp(S_{1v}^f/k)\exp(-E_{1v}^f/k\bar{T}_a), \quad (13)$$

$$c_{2v}^0=6(c_{1v}^0)^2\exp(-S_{2v}^b/k)\exp(E_{2v}^b/k\bar{T}_a), \quad (14)$$

$$E_{2v}^b=2E_{1v}^f-E_{2v}^f, \quad (15)$$

$$S_{2v}^b=2S_{1v}^f-S_{2v}^f, \quad (16)$$

$$c_{1v}=\frac{[1+48c_t\exp(-S_{2v}^b/k)\exp(E_{2v}^b/k\bar{T}_a)]^{1/2}-1}{24\exp(-S_{2v}^b/k)\exp(E_{2v}^b/k\bar{T}_a)}, \quad (17)$$

[30] C. P. Flynn, Phys. Rev. **133**, A587 (1964); **134**, A241 (1964).
[31] R. W. Balluffi and D. N. Seidman, J. Appl. Phys. **36**, 2708 (1965).

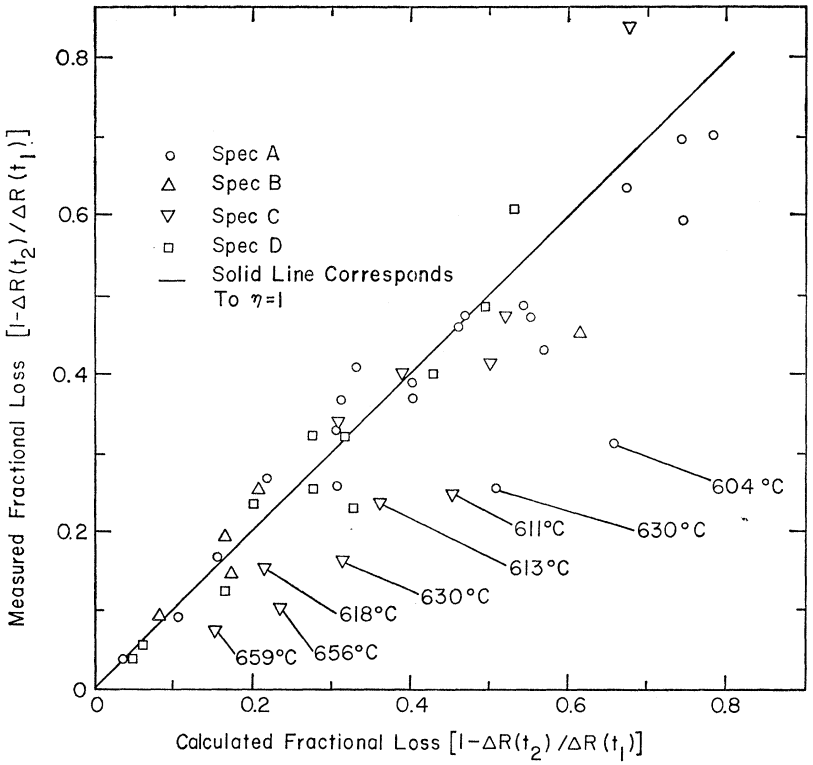

FIG. 13. Experimentally measured fractional vacancy loss at $\bar{T}_a$ versus the calculated fractional vacancy loss for specimens A, B, C, and D. The calculated fractional loss was obtained using the present diffusion limited monovacancy-divacancy annealing model with dislocations as sinks and with the parameters listed in Table II. The solid line with unit slope corresponds to a dislocation climb efficiency η of unity.

$$c_{2v}=6c_{1v}^2\exp(-S_{2v}{}^b/k)\exp(E_{2v}{}^b/k\bar{T}_a), \quad (18)$$

$$D_{1v}=D_{01v}\exp(-E_{1v}{}^m/k\bar{T}_a), \quad (19)$$

$$D_{2v}=D_{02v}\exp(-E_{2v}{}^m/k\bar{T}_a). \quad (20)$$

Here, c_t is the total concentration of vacant sites, $c_{1v}{}^0$ and $c_{2v}{}^0$ are the thermal equilibrium concentrations of monovacancies and divacancies, respectively, the $E_{nv}{}^f$'s are formation energies, the $S_{nv}{}^f$'s are formation entropies, $E_{2v}{}^b$ is the divacancy binding energy, $S_{2v}{}^b$ is the divacancy binding entropy, and the $E_{nv}{}^m$'s are migration energies. It is seen that the following eight defect constants must be specified in this model: $S_{1v}{}^f$, $D_{1v}{}^f$, $S_{2v}{}^b$, $E_{2v}{}^b$, D_{01v}, D_{02v}, $E_{1v}{}^m$, and $E_{2v}{}^m$. In addition, N_d must be determined for each specimen. Our problem, therefore, is to fit the model, with its eight constants, to the experimental data listed above under (i), (ii), and (iii).

The calculations required to obtain a fit to the data under (i) were obtained by assuming that the quasi-steady-state equation (11) held instantaneously at all times during the annealing and integrating it over the thermal history of each run. Various test sets of the parameter values were assumed and the total defect loss (i.e., the decrease in c_t) during each annealing run over its measured temperature-time history was calculated with a computer from Eq. (11) in second-order finite difference form.

The comparatively simple calculations required to obtain a fit to the data under (ii) were carried out by using Eqs. (12), (13), and (18).

The calculations required to obtain a fit to the data under (iii) employed the following equation which expresses the over-all tracer self-diffusion coefficient D^{sd} in terms of the contributions from the monovacancies and divacancies ($D_{1v}{}^{sd}$ and $D_{2v}{}^{sd}$, respectively):

$$D^{sd}=D_0{}^{sd}\exp(-Q/kT)=D_{1v}{}^{sd}+D_{2v}{}^{sd}, \quad (21)$$

where $D_0{}^{sd}$ is the isotope self-diffusion preexponential factor and Q is the activation energy for tracer diffusion. For isotope diffusion in a face-centered cubic lattice $D_{1v}{}^{sd}$ and $D_{2v}{}^{sd}$ are given by[32]

$$D_{1v}{}^{sd}=D_{01v}\exp(-E_{1v}{}^m/kT)c_{1v}{}^0\xi_{1v} \quad (22)$$

and

$$D_{2v}{}^{sd}=4D_{02v}\exp(-E_{2v}{}^m/kT)c_{2v}{}^0\xi_{2v}, \quad (23)$$

where $\xi_{1v}=0.781$ and $\xi_{2v}=0.54$ are the correlation factors[33] for monovacancies and divacancies, respectively.

The best values of the eight parameters required to fit the model to all of the data under (i), (ii), and (iii) were determined by carrying out a large number of computer calculations in which the parameters were systematically varied until a self-consistent best fit to all the data was obtained. In the process a single best value for the apparent dislocation density of each specimen was obtained (these best dislocation density values are listed in Table I). In order to begin the calculations $E_{2v}{}^m$ was set equal to 0.69 eV. This value

[32] R. O. Simmons and R. W. Balluffi, Phys. Rev. **117**, 52 (1960).
[33] K. Compaan and Y. Haven, Trans. Faraday Soc. **52**, 786 (1956); G. Schottky, Phys. Letters **12**, 95 (1964).

was equal to the apparent value of E^m found earlier in Sec. III B for low-temperature annealing at $T_a<500°C$ and was also consistent with the value $E^m=0.71\pm0.03$ eV found earlier by others at still lower temperatures near room temperature. It was also recognized immediately that a rather large binding energy would be required in order to allow this divacancy to make significant contributions to the annealing rate at temperatures as high as 400–500°C.

The calculations showed that the allowed ranges of variation of the values of the eight model parameters were very *severely* restricted by the experimental data under (i), (ii), and (iii). The experimental data were therefore sufficient to resolve rather sharply the parameters of the model. The final best values of the model parameters are given in Tables I and II. The fits to the data under (i), (ii), and (iii) are shown in Figs. 13, 7, and 12, respectively, and it is seen that the model fits the data quite well. In Figs. 7 and 12 excellent fits to the data were obtained which are well within expected experimental error. The results in Fig. 13 show quite satisfactory agreement between the calculated fractional defect losses and measured defect losses during annealing between t_1 and t_2 at annealing temperatures below $\bar{T}_a\simeq600°C$. However, the measured fractional loss is seen to be lower than the calculated fractional loss at the high temperatures, i.e., $\bar{T}_a\gtrsim600°C$ (see indicated data points and Sec. III D for further discussion of this point).

Finally, we may justify the assumption of our model that the monovacancies and divacancies maintained instantaneous local equilibrium with each other during the course of the present experiments. Balluffi and Siegel[17] have given an expression for the relaxation time $\theta(T_q,T_a)$ which is required for a closed monovacancy-divacancy system initially at equilibrium at T_q to reach e^{-1} of its new equilibrium distribution at T_a after an infinitely fast quench from T_q to T_a. Values of θ (700°C,T_a) were calculated for different values of T_a in the range 200–600°C and for different values of $E_{2v}{}^b$ using a model where all other parameters had the values of the present model given in Table II. The results are shown in Fig. 14. It is noted that the relaxation times[34] are much shorter than the times required for any appreciable defect annealing.

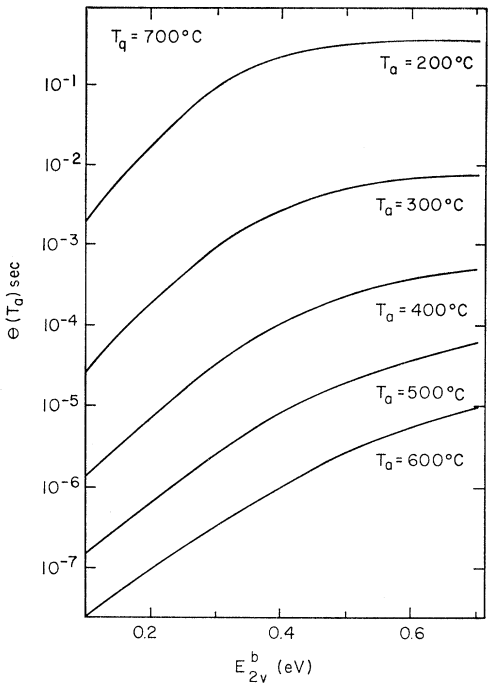

FIG. 14. Calculated relaxation time $\theta(T_a)$ versus divacancy binding energy $E_{2v}{}^b$. The parameter $\theta(T_a)$ is the time for a closed monovacancy-divacancy system initially at T_q to reach e^{-1} of its new equilibrium distribution at T_a after an infinitely rapid quench from T_q. All necessary parameters needed in the calculation taken from Table II.

D. Dislocations as Sinks

All the analyses and interpretations in the preceding sections were based on the assumption that the dominant sink for the excess vacancies during the nearly isothermal region III ($\bar{T}_a$) was the three-dimensional dislocation network. Additional possible vacancy sinks were the free surfaces, grain boundaries, and any subgrain walls (dense planar arrays of dislocations). Therefore, it was necessary to demonstrate that the free dislocations actually were the dominant sinks at $\bar{T}_a$. This was accomplished by measuring the densities of these additional sinks and then calculating the isothermal mean fractional vacancy loss $[L(t)]$,

$$L(t)=1-[\bar{c}_t(t)-c_t{}^0(T_a)]/[c_t{}^0(T_q)-c_t{}^0(T_a)], \quad (24)$$

as a function of time at T_a after a quench from T_q for all the sinks. Since there was no simple analytical expression available which could be used to describe the simultaneous diffusion of vacancies to two or more different types of sinks, the diffusion equation was simply solved for each of the four possible sinks under the assumption that each sink in turn was the only operative sink. In this manner we obtained an upper bound on $L(t)$ for each possible sink.[35] The results of these calculations are presented in Fig. 19 for an isothermal anneal at 300°C ($D_{2v}=3.11\times10^{-9}$ cm^2 sec^{-1}) using the sink data listed in Table IV.

It is seen that for the range of dislocation densities found in the present experiments that the three-dimensional dislocation network dominated the high-temperature annealing kinetics, with the exception of a short initial time period during which there was a transient vacancy flux to the other sinks. This initial transient in no case exceeded $\sim10\%$, and since the isothermal anneals ($\bar{T}_a$) began with a fractional loss of

[34] Since the quenching rate was assumed to be infinitely fast, the calculated relaxation time from this expression is the *upper bound* on the actual time, since for any finite quenching rate some redistribution will occur during the quench.

[35] See Appendix B for the details of these calculations.

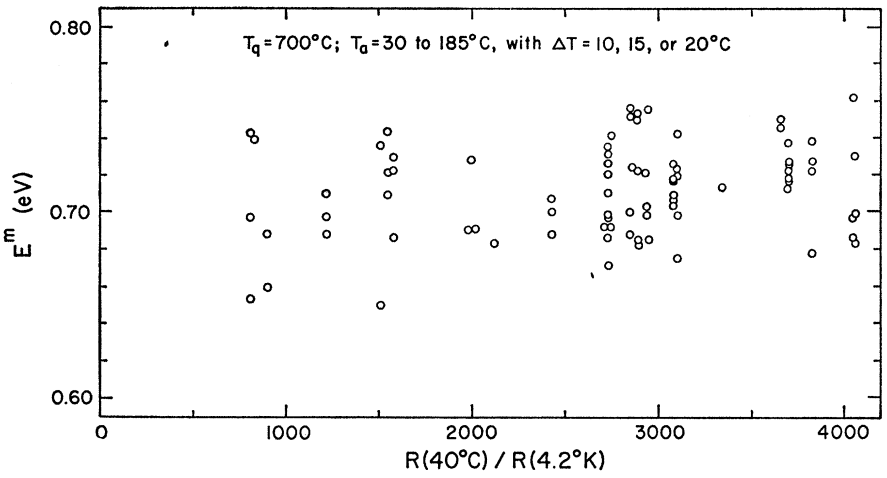

FIG. 15. Defect migration energy by the change of slope method as a function of base resistance ratio ℜ for various gold wire specimens quenched from T_q=700°C and annealed in the temperature range 30–185°C. Data from unpublished work of Ytterhus (Ref. 38).

~5 to 10% this transient was most likely completed at the start of each anneal.

We also note that the magnitudes of the dislocation densities calculated on the basis of our annealing model (see Table I) are in good general agreement with the dislocation densities measured directly by Seidman and Balluffi[19] in their previous work with well annealed and quenched gold specimens. These densities appear to be characteristic of such gold specimens subjected to the present treatments.

The use of the diffusion limited dislocation annealing model in the present work was further justified by considering the earlier work of Seidman and Balluffi[19] on the efficiency of the dislocation climb process in gold. In these experiments the complete sink structure of each specimen was determined experimentally, and the measured fractional losses during the down-quench were then compared with the fractional losses calculated on the basis of a diffusion limited dislocation model with a temperature- (time-) dependent diffusion coefficient. For $\bar{T}_q$=653°C the calculated maximum loss of 8% agreed within 3% with the measured loss for a specimen with a *measured* dislocation density of 6.5×10^7 cm cm^{-3}. Thus, the general conclusion that can be reached as a result of the previous work, as well as the present work, is that the three-dimensional dislocation network in gold behaves as an efficient high-temperature sink for supersaturated vacancies.

TABLE IV. Sink data for specimens used in present investigation.

Specimen	Grain size diam (cm)[a]	Length[b] (cm)	Subgrain[c] diam (cm)	Dislocation density (cm^{-2})[d]
A	0.0127	0.0109	0.0064	8.3×10^6
D	0.0127	0.0138	0.0064	5.1×10^7
F	...	...	...	6.5×10^6

[a] The wire specimens employed in these experiments had an essentially bamboo-type grain structure. Hence, the grain diameter was taken as the wire diameter.
[b] Measured with an optical metallograph.
[c] We were unable to measure the subgrain diameter, hence we took it to be one-half the grain diameter. This is not an unreasonable estimate (e.g., see experimental measurements of Seidman and Balluffi, Ref. 19) of the maximum subgrain size.
[d] See Table I.

However, some dropoff in the sink efficiency seemed to occur at the very highest annealing temperatures as seen in Fig. 13. For $\bar{T}_a$ greater than about 600°C, the experimentally measured fractional losses during annealing were lower than the losses calculated on the assumption of perfect line sinks, indicating some decrease of the dislocation sink efficiency.

These results can be understood on the basis of previous work by Seidman and Balluffi,[19] who have characterized the climb process by the climb efficiency parameter η, which is defined as

$$\eta=\frac{\text{observed climb rate}}{\text{calculated climb rate if diffusion-limited}}, \quad (25)$$

so that $\eta=1$ corresponds to the maximum possible climb rate. The chemical potential (μ_v) of the supersaturated vacancies is related to the driving force for climb (F_c) by the relationship

$$F_c=\frac{g}{b^2}|\mu_v|, \quad (26)$$

where g is a dimensionless geometric factor, b is the Burgers vector, and $|\mu_v|$ is given by

$$|\mu_v|=kT_a\left|\ln\left\{\left(\frac{\bar{c}-c^0}{c^0}\right)+1\right\}\right|, \quad (27)$$

where c^0 is the local equilibrium value and $\bar{c}$ is the mean vacancy concentration. The concentration $\bar{c}$ is the relevant quantity[36] to be used in the calculation of $|\mu_v|$, since the change in the mean vacancy concentration determines the net decrease in the free energy, and hence the amount of work that becomes available to cause climb. On very general thermodynamic grounds, as well as on the basis of detailed kinetic models (see Thomson and Balluffi[37]), we expect η to

[36] Equation (27) was misprinted in Ref. 19 where it was also erroneously stated that $|\mu_v|$ was determined by the magnitude of the deviation of the point-defect concentration from local equilibrium.
[37] R. M. Thomson and R. W. Balluffi, J. Appl. Phys. 33, 803 (1962); R. W. Balluffi and R. M. Thomson, *ibid.* 33, 817 (1962).

TABLE V. Summary of different investigations in which a defect migrating with E^m near 0.70 eV has been observed.

Investigator	Nominal purity	Resistivity ratio (annealed state)	Concentration range	Temperature range	E^m(eV)
1. Ytterhus and Balluffi[a]	99.999	900–4000	1.5×10^{-6}–50×10^{-6}	30–185°C	0.71
2. Siegel[b]	99.999 and 99.9999	529–22 500	2.2×10^{-6}–28×10^{-6}	40–100°C	0.70
3. Kauffman and Meshii[c]	>99.999	2500–4000	0.7×10^{-6}–100×10^{-6}	···	0.71
4. Mori, Meshii, and Kauffman[d]	>99.999	>2000	50×10^{-6}	···	0.69
5. Delaplace *et al.*[e]	99.999	380	$<\sim40\times10^{-6}$	75–100°C	0.70
6. Emrick[f]	99.999	···	···	300–440°C	0.67
7. Present work	99.999 and 99.9999	3287–7849	$<30\times10^{-6}$	160–483°C	0.69

[a] See Ref. 7. [b] See Ref. 8. [c] See Ref. 6. [d] See Ref. 5. [e] See Ref. 9. [f] See Ref. 10.

decrease with a decrease in the driving force for climb.

As seen in Fig. 13, η remained at unity for $T_a<\simeq600$°C and then decreased to lower values which did not fall below $\eta\simeq0.47$ at the higher annealing temperatures. According to Eqs. (26) and (27) the defect chemical potential and the climb driving force decreased with increased annealing temperature, since the supersaturation $(\bar{c}-c^0)/c^0$ decreased. Use of these relations shows that η became less than unity when $|\mu_v|$ dropped below about 0.1 eV. This indicates that a driving defect chemical potential of about 0.1 eV was necessary to achieve a climb efficiency of unity. This result is consistent with the previous results of Seidman and Balluffi[19] where it was shown in up-quenching experiments with gold that the climb efficiency seemed to decrease when the subsaturation decreased sufficiently.

IV. DISCUSSION

The most interesting result of the present work is the consistency of the data with a tightly bound divacancy having a migration energy close to 0.69 eV. Our results are quite consistent with earlier work at lower temperatures. This defect has now been observed in at least seven different investigations as seen in Table V. The results summarized there offer impressive evidence that this defect makes an important contribution to the annealing over a wide range of conditions including a range of defect concentration of about two orders of magnitude and a temperature range extending between 30 and about 400°C. This temperature range is now as extensive as the range for which the tracer self-diffusion activation energy Q has been determined (see Table III). The migration energy of about 0.69 eV appears to be independent of nominal specimen purity over a considerable range as indicated by the varying resistivity ratios $\mathfrak{R}$ achieved in the investigations listed in Table V. Previously unpublished evidence for the lack of any purity dependence is seen in Fig. 15, where some data of Ytterhus[38] show the migration energy to remain constant over a large range of $\mathfrak{R}$ values. It is also emphasized that the migration energy of about 0.69 eV has been observed during annealing to a variety of sinks which include black-spot vacancy precipitates[7,8] and dislocation loops,[8] stacking fault tetrahedra,[7,8] and dislocations.[7,38] These results indicate that this observed migration energy must be independent of the sink properties. Finally, it is noted that this migration energy has also been obtained by a variety of techniques for determining migration energies which include the change-of-slope method,[5–9] the Palmer method,[7] the standard Arrhenius method,[9,38] and the methods of the

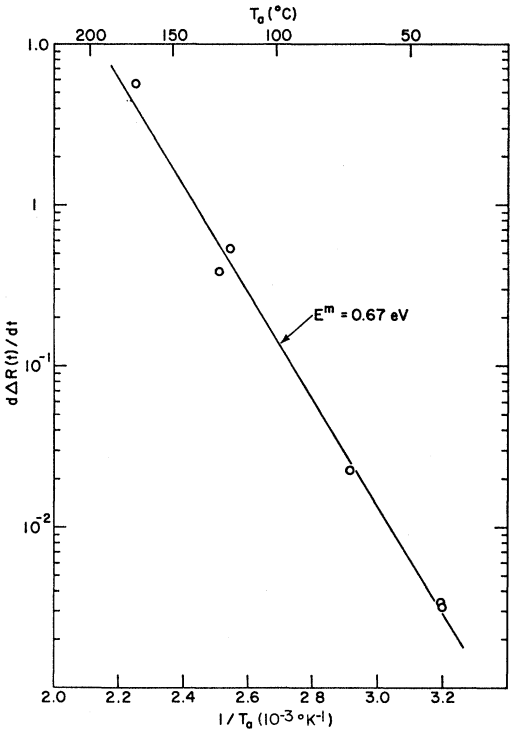

FIG. 16. Arrhenius plot of defect annealing rate versus T_a^{-1} based on unpublished data of Ytterhus (Ref. 38). The annealing rate at the point where 42% of the initial concentration was annealed is plotted versus T_a^{-1} over the temperature range 40–170°C for a series of specimens with matched base resistance ratios $\mathfrak{R}$ and therefore a common sink density (see Ref. 39 for details). The plot yielded an activation energy of 0.67 eV.

[38] J. A. Ytterhus, Ph.D. thesis, University of Illinois, 1964 (unpublished).

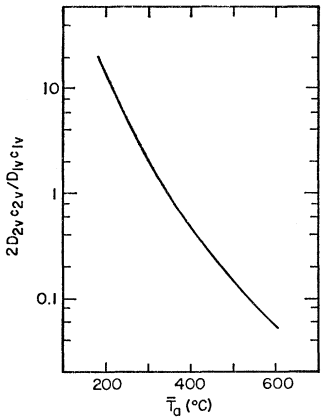

FIG. 17. The calculated ratio of the flux carried by divacancies ($2D_{2v}c_{2v}$) to that carried by monovacancies ($D_{1v}c_{1v}$) versus $\bar{T}_a$ for the present monovacancy-divacancy model. Calculations made for $\bar{T}_a=700$°C with the parameters listed in Table II.

present work. Previously unpublished results of Ytterhus[38] are shown in Fig. 16 which demonstrate the determination of $E^m=0.67$ eV by applying the Arrhenius method to some of his data. In Fig. 16 the log of the instantaneous annealing rate at the point where 42% of the increment was annealed is plotted versus T_a^{-1} for a set of matched specimens with the same sink density (as evidenced by a fixed value of $\mathfrak{R}$ in these particular experiments). Furthermore, the annealing rate in each case was measured under quasi-steady-state conditions so that the results could not have been affected by transients which can conceivably affect measurements of E^m in the sudden-change-of-slope method.[17] Taken altogether, the above results constitute strong evidence for a defect which migrates with $E^m\simeq 0.69$ eV.

The divacancy binding energy of 0.4 eV is higher than that predicted by several previous investigators. However, we are not aware of any strong *a priori* reasons why the value $E_{2v}{}^b=0.4$ eV should be considered as unreasonably high. The small binding entropy $S_{2v}{}^b=-0.093k$ (Table II) indicates that the divacancy formation entropy is only slightly larger than the combined entropies of two monovacancies. We note that these results differ considerably from those of Schottky *et al.*,[39] who *calculated* a considerably more negative binding entropy (i.e., $S_{2v}{}^b=-2.2k$) and then proceeded to extract a small binding energy (i.e., $E_{2v}{}^b=0.1$ eV) on the basis of their interpretation of various experimental data. The use of this large negative calculated binding entropy ($S_{2v}{}^b$) *predetermines* the outcome of their result in a monovacancy-divacancy annealing model, since it is impossible to have both $S_{2v}{}^b$ and the divacancy binding energy large and still obtain agreement with the self-diffusion data and the equilibrium vacancy concentration measurements. Our data yielded a divacancy diffusivity given by

$$D_{2v}=3.65\times10^{-3}\times\exp(-0.69/kT). \quad (28)$$

[39] G. Schottky, Z. Physik **159**, 584 (1960); G. Schottky, A. Seeger, and G. Schmid, Phys. Status Solidi **4**, 419 (1964).

It is encouraging to note that this result is in good agreement with the value

$$D_{2v}=4.90\times10^{-3}\times\exp(-0.70/kT) \quad (29)$$

which was determined by Siegel[8] on an absolute basis by means of a completely independent experiment and technique. In his work Seigel measured the electrical-resistivity annealing kinetics of the vacancy defects to sinks whose geometry was accurately measured by transmission electron microscopy. These data allowed the defect diffusivity to be calculated directly.[40] The values of the preexponential frequency factors for the monovacancy and divacancy diffusivities (Table II) which are in the range 10^{13} sec^{-1} seem quite reasonable. The frequency value for the more relaxed and "looser" divacancy is seen to be smaller than that for the monovacancy as should be the case. The remaining values of the defect parameters in Table II appear to be quite normal. The present result, suggesting a tightly bound divacancy, requires that the divacancy make a significant contribution to the equilibrium vacancy defect population and to the self-diffusivity at temperatures approaching the melting point. In fact, $2c_{2v}{}^0/c_t{}^0=0.20$ and $D_{2v}{}^{sd}/D^{sd}=0.102$ at 1333°K. At 1000°K, $2c_{2v}{}^0/c_t{}^0=0.05$ and $D_{2v}{}^{sd}/D^{sd}=0.041$. Using the model parameters in Table II we may also calculate the importance of the divacancy annealing flux relative to the monovacancy annealing flux as a function of annealing temperature. These results are shown in Fig. 17 for the quasi-steady-state annealing situation directly after quenching from 700°C. The divacancy and monovacancy annealing fluxes are equal at about 350°C and the divacancy becomes predominant at lower temperatures. This result poses the question of why the divacancy with $E_{2v}{}^m=0.69$ eV appeared to dominate the annealing at temperatures as high as 483°C (Figs. 8–11). The answer is given by Fig. 18, where we have plotted ($D_{1v}c_{1v}+2D_{2v}c_{2v}$) versus $1/T$(°K) for the quasi-steady-state situation directly after quenching from 700°C. It is seen that the quantity $D_{1v}c_{1v}+2D_{2v}c_{2v}$, which is proportional to the total annealing flux, can be fairly well represented by $A\exp(-E^m/kT)$, where $E^m=0.69$ for small fractions annealed, but that a definite curvature is present for large fractions annealed (e.g., 80% annealed). An examination of Figs. 8 and 9 shows that the majority of our annealing runs were at fractional losses which were less than 50% (with the exception of two points), and, since in each case we measured the integrated fractional loss, the points are further biased towards a small net fractional loss. This rather fortuitous result arises from the way in which the variations of the D_{nv} and c_{nv} with temperature combine over the limited temperature range (340°C) in question. We may conclude that the earlier results in Sec. III B indicating apparent consistency up to $T_a=500$°C with

[40] It is noted that the value of D_{2v} given in Eq. (29) differs somewhat from that presented in Ref. 8. This is the result of a further analysis of the data in Ref. 8 which is being prepared for publication.

a single defect with $E^m=0.69$ eV were largely fortuitous. This result shows clearly the danger of analyzing defect annealing kinetics over a restricted temperature range on the basis of simple assumptions.

We emphasize finally that the available experimental results are, of course, not completely sufficient to establish firmly the present model. However, the results summarized in Table V indicate strongly that some type of rather tightly bound vacancy cluster is very important in gold. If this defect is not the divacancy as assumed here, then it may conceivably be the trivacancy. Presumably, a model involving the trivacancy built along lines similar to the above monovacancy-divacancy model could be produced. It is interesting to note that the tightly bound clusters with $E^m=0.69$ eV cannot have too strong a binding with each other, or else rapid homogeneous vacancy-defect precipitation would occur due to their collisions with the subsequent formation of large immobile vacancy clusters. It is known that this does not occur in quenched gold even at low annealing temperatures. Instead, vacancy precipitation occurs on a coarse scale at heterogeneous nucleation sites.[8] We therefore must always require at least one relatively weak link in the binding scheme for the chain of vacancy clustering events which could lead to the formation of large immobile vacancy precipitates. It is also noted that the monovacancy-divacancy model assumed above does not provide any simple and unique explanation for the slight dropoff in E^m which has been observed in previous work[7] near room temperature at defect concentrations higher than those attained in the present work. In the previous work values of E^m as low as $\simeq$0.63 eV were obtained by the change-of-slope method at concentrations approaching $c_t\simeq 3\times 10^{-4}$. In those experiments the defect annihilation occurred mainly at stacking-fault tetrahedra which nucleated and grew during annealing. It seems possible that effects due to transients accompanying the rapid temperature change in the change-of-slope method and factors connected with the nucleation and growth of the tetrahedron sinks could have affected the values of E^m. Further experiments involving the determination of E^m over a wider range of temperature and concentration are presently in progress in our laboratory.

Finally, we note that we have not attempted to take into account any temperature variations of the formation and migration energies of the vacancy defects in our analysis. Presumably such effects could be at least partially responsible for the lack of agreement between the high- and low-temperature data in a simple one-defect model. In fact, Stoebe and Dawson[41] have recently argued that there is a large temperature dependence of the monovacancy migration energy in both gold and aluminum and that high-temperature diffusion data and low-temperature quenching and annealing data should not be compared without first suitably correcting for this effect. In our opinion the large temperature dependence of $E_{1v}{}^m$ suggested by Stoebe and Dawson is not established at present. Their conclusion is based heavily on their procedure of combining the self-diffusion measurements of a limited number of investigators to produce over-all Arrhenius plots with upward curvature near the melting point. It is interesting to note in this respect that the data of no single investigation show a large upward curvature. Furthermore, a recent theoretical estimate[42] of the temperature dependence of $E_{1v}{}^f+E_{1v}{}^m$ predicts only a small effect which is about the size of the experimental uncertainty of the present work.

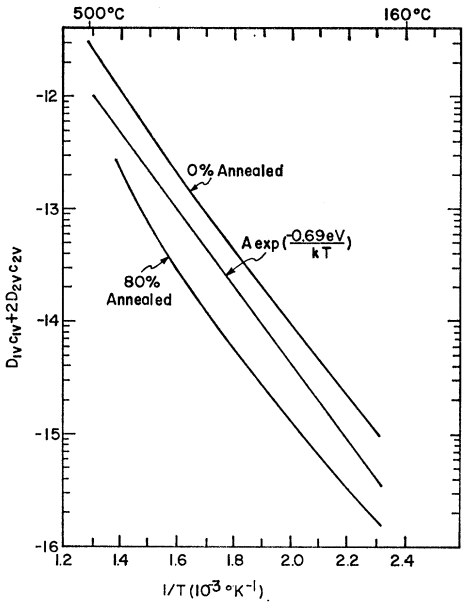

FIG. 18. The calculated parameter $D_{1v}c_{1v}+2D_{2v}c_{2v}$ versus $1/T$(°K) for the quasi-steady-state situation directly after quenching from 700°C for 0% annealed and 80% annealed compared with the expression $A\exp(-E^m/kT)$ with $E^m=0.69$ eV.

ACKNOWLEDGMENTS

We would like to thank R. Conkling of Infotec, Inc., Westbury, Long Island, N. Y., who designed and built our rapid data acquisition system, and Professor R. W. Siegel for several interesting discussions and for his unpublished recomputed value of the divacancy diffusion coefficient.

APPENDIX A: MEASURING AND RECORDING SYSTEM

In the following, we present a detailed discussion of the principles of the measurement of the temperature-time function $T(t)$ and of the recording system used to obtain the required experimental data.

The basic method involved the simultaneous measurement of the dc potential drops across the specimen and a standard laboratory resistor in series with the

[41] T. G. Stoebe and H. I. Dawson, Phys. Rev. **166**, 621 (1968).

[42] A. S. Nowick and G. J. Dickes, Phys. Status Solidi **24**, 461 (1967).

specimen. Therefore, the resistance of the specimen relative to that of the standard resistor (as a function of time) was given by

$$\frac{R_{\text{spec}}(t)}{R_{\text{std}}(t)}=\left[\frac{V_{\text{spec}}(t)}{V_{\text{std}}(t)}\right]\left[\frac{I_{\text{std}}(t)}{I_{\text{spec}}(t)}\right], \tag{A1}$$

where R, V, and I denote resistance, voltage, and current, respectively. The resistance value of the standard resistor was chosen such that the Joule heating did not change its value to within one part in 10^5 for the specimen heating currents employed, and thus its value was independent of time. In addition, the two potential measurements were made simultaneously. Hence, the instantaneous currents through the specimen and the standard resistor were identical. Therefore, Eq. (A1) reduced to

$$\frac{R_{\text{spec}}(t)}{R_{\text{std}}(t)}=\frac{V_{\text{spec}}(t)}{V_{\text{std}}(t)}. \tag{A2}$$

The standard resistance ratio $R_{\text{spec}}(t)/R_{\text{spec}}(40°\text{C})$ was then obtained by means of the relationship

$$\frac{R_{\text{spec}}(t)}{R_{\text{spec}}(40°\text{C})}=\left[\frac{V_{\text{spec}}(t)}{V_{\text{std}}(t)}\right]\left[\frac{R_{\text{std}}'}{R_{\text{std}}}\right]\left[\frac{V_{\text{std}}'}{V_{\text{spec}}(40°\text{C})}\right], \tag{A3}$$

where the primes[43] denote the values of R and V for the measurement at 40°C. The specimen temperature was then obtained from the ratio in Eq. (A3) by employing the normalized resistance-versus-temperature data of Meechan and Eggleston.[12]

As shown above, the principle function of the apparatus was to measure and store the time-dependent voltage ratio $V_{\text{spec}}(t)/V_{\text{std}}(t)$ in Eq. (A3). Two basically different types of voltage measurements were made during a thermal cycle. The first type of measurement was made during the transient regions II and IV (see Fig. 1) when the power supply in the specimen heating and quenching circuit was switched to a low voltage level. The second type of measurement was a differential one and was made during the steady-state temperature regions at the quench temperature (region I) and the annealing temperature (region III).

The voltage measurements made during the transient periods II and IV were accomplished using two wide-band Dana 3400 amplifiers (denoted amp 1 and amp 2 in Fig. 4). These amplifiers amplified the rather small input signal during the transient regions and also served to isolate the analog ground from the specimen heating and quenching circuit. This isolation was necessary since the voltages generated across the specimen and standard resistor were floating potentials and the amplifiers had to convert these floating inputs to a common ended ground for measurement. The differential measurements during the steady temperature regions were made using two Dana 3500 amplifiers (marked diff amp 1 and diff amp 2 in Fig. 4) in conjunction with a precision voltage dividing network and a very stable 10 VDC reference standard (ROTEC 410). Thus, the two differential amplifiers (diff amp 1 and diff amp 2) measured only the difference between the amplified voltage drops and the preset potentials. Hence, the voltages recorded during the steady-state temperature regions were variations from the fixed reference voltages. The reference voltages were determined by the desired annealing temperature $\bar{T}_a$ prior to a run. This technique gave the measuring system an effective resolution of five significant figures in the steady-state temperature regions.

The measured analog voltages were then routed to an analog to digital converter (A/D) via a four-channel analog switch. The voltages were next converted into digital form and subsequently stored in a magnetic storage unit. The capacity of this storage unit was 1024 voltage ratios. Therefore, each quench and annealing run consisted of a maximum of 1024 individual temperature measurements distributed between the four regions (I through IV).

The apparatus logic was used to control the heating current in the specimen circuit, the voltage inputs, the A/D converter, the magnetic storage unit, and finally the output paper tape punch. The specimen heating and quenching circuit was a slave to the system's logic since the heating current was switched to the proper level by a pulse generated by the system. The master clock for the base of the system's logic was a 2 kc/sec crystal-controlled oscillator.[44] This clock was variable from 2000 to 15.625 cps in eight frequency steps.

At the end of a run the pertinent experimental conditions were inserted into the tape record via the paper-punch format control. Finally, the paper tape punch was used to unload the data that were stored in the magnetic memory unit. This paper tape record was then converted into magnetic tape which was subsequently used for all the data processing.

APPENDIX B: SOLUTION OF THE DIFFUSION EQUATION FOR ANNEALING LOSSES AT THE FOUR POSSIBLE VACANCY SINKS

The expressions used to calculate the losses to the various sinks are given below. For all cases considered the assumption was made that the specimen was quenched infinitely fast from T_q where the total equilibrium vacancy concentration was $c_t^0(T_q)$ and then annealed at T_a where the total equilibrium vacancy concentration was $c_t^0(T_a)$, and also that the sink in

[43] The high-temperature annealing experiments employed a 0.01-Ω resistor while the 40°C measurements employed a 1-Ω resistor. Both were Leeds and Northrup standard resistors accurate to one part in 10^5.

[44] The system has also been used with a basic clock frequency of 4 kc/sec employing an external oscillator. The 4-kc/sec signal provided a temperature point once every 0.25 msec. This sampling rate was particularly useful during the transition regions II and IV.

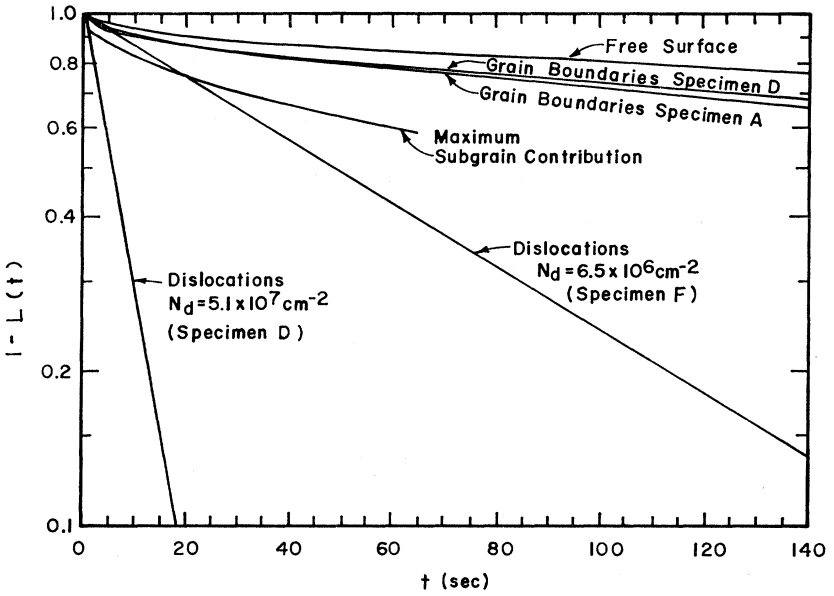

FIG. 19. The quantity $[1-L(t)]$ versus annealing time at 300°C for the various types of sinks present in the specimens employed in the present work (see Table IV). Here $L(t)$ is the fractional defect loss and $D=D_{2v}=3.11\times10^{-9}$ cm^2 sec^{-1}. The fractional loss at each sink was calculated on the assumption that each given sink acted independently of the other sinks. Hence, the curves represent upper bounds on the fraction of vacancies lost to a given type of sink.

question maintained local defect equilibrium in its vicinity during the course of the entire anneal. It was further assumed that only one defect was present in the system.

1. Annealing to Dislocations

This solution was obtained by integrating Eq. (11) with a constant D_{2v}, $D_{1v}=0$, and $2c_{2v}=c_t$, and is given by

$$L(t)=1-\exp\left\{\frac{2\pi N_d D_{2v}t}{\ln[r_d(\pi N_d)^{1/2}]}\right\}. \tag{B1}$$

The effects of the dislocation climb motion on the annealing rate have been shown by Balluffi and Seidman[31] to be negligible.

2. Annealing to the Free Surfaces

We employed an infinitely long right circular cylinder of radius a as our model, since the specimens were in the form of wires. The short time solution for the mean fractional vacancy loss is then[45]

$$L(t)\cong\frac{4}{\pi^{1/2}}\left(\frac{D_{2v}t}{a^2}\right)^{1/2}+\left(\frac{D_{2v}t}{a^2}\right) \tag{B2}$$

for the values of $(D_{2v}t/a^2)$ used to calculate Fig. 19.

3. Annealing to Grain Boundaries

The model chosen for the grains was a right circular cylinder of radius a and length l. The solution in this case is given as the product of the solution for the case of diffusion in an infinitely long right circular cylinder and diffusion in a slab of thickness l. Hence, the loss for small time is given by[45]

$$L(t)\cong\left[\frac{2}{\pi^{1/2}}\left(\frac{D_{2v}t}{l^2}\right)^{1/2}+\frac{4}{\pi^{1/2}}\left(\frac{D_{2v}t}{a^2}\right)^{1/2}+\frac{D_{2v}t}{a^2}-\frac{2}{\pi^{1/2}}\left(\frac{D_{2v}t}{l^2}\right)^{1/2}\right]\left[\frac{4}{\pi^{1/2}}\left(\frac{D_{2v}t}{a^2}\right)^{1/2}+\frac{D_{2v}t}{a^2}\right]. \tag{B3}$$

4. Annealing to Subgrain Walls

We chose a sphere of radius r as a model for the subgrains. Hence, the solution for small times is given by[45]

$$L(t)\cong\frac{6}{\pi^{1/2}}\left(\frac{D_{2v}t}{r^2}\right)^{1/2}+3\left(\frac{D_{2v}t}{r^2}\right). \tag{B4}$$

[45] H. S. Carslaw and J. C. Jaeger, *Conduction of Heat in Solids* (Oxford University Press, London, 1959).